Combined TRPC3 and TRPC6 blockade by selective small-molecule or genetic deletion inhibits pathological cardiac hypertrophy

Kinya Seo[a,1], Peter P. Rainer[a,b,1], Virginia Shalkey Hahn[a,1], Dong-ik Lee[a], Su-Hyun Jo[a,c], Asger Andersen[d], Ting Liu[a], Xiaoping Xu[e], Robert N. Willette[e], John J. Lepore[e], Joseph P. Marino, Jr.[e], Lutz Birnbaumer[f], Christine G. Schnackenberg[e], and David A. Kass[a,2]

[a]Division of Cardiology, Department of Medicine, Johns Hopkins Medical Institutions, Baltimore, MD 21205; [b]Division of Cardiology, Department of Medicine, Medical University of Graz, 8036 Graz, Austria; [c]Department of Physiology, Institute of Bioscience and Biotechnology, Kangwon National University School of Medicine, Chuncheon 200-701, South Korea; [d]Department of Cardiology, Aarhus University Hospital, 8200 Aarhus, Denmark; [e]GlaxoSmithKline Heart Failure Discovery Performance Unit, King of Prussia, PA 19406; and [f]Laboratory of Neurobiology, National Institute of Environmental Health Sciences, Research Triangle Park, NC 27709

Edited by Christine E. Seidman, Howard Hughes Medical Institute, Harvard Medical School, Boston, MA, and approved December 19, 2013 (received for review May 13, 2013)

Chronic neurohormonal and mechanical stresses are central features of heart disease. Increasing evidence supports a role for the transient receptor potential canonical channels TRPC3 and TRPC6 in this pathophysiology. Channel expression for both is normally very low but is increased by cardiac disease, and genetic gain- or loss-of-function studies support contributions to hypertrophy and dysfunction. Selective small-molecule inhibitors remain scarce, and none target both channels, which may be useful given the high homology among them and evidence of redundant signaling. Here we tested selective TRPC3/6 antagonists (GSK2332255B and GSK2833503A; IC_{50}, 3–21 nM against TRPC3 and TRPC6) and found dose-dependent blockade of cell hypertrophy signaling triggered by angiotensin II or endothelin-1 in HEK293T cells as well as in neonatal and adult cardiac myocytes. In vivo efficacy in mice and rats was greatly limited by rapid metabolism and high protein binding, although antifibrotic effects with pressure overload were observed. Intriguingly, although gene deletion of TRPC3 or TRPC6 alone did not protect against hypertrophy or dysfunction from pressure overload, combined deletion was protective, supporting the value of dual inhibition. Further development of this pharmaceutical class may yield a useful therapeutic agent for heart disease management.

ion channels | calcium | nuclear factor of activated T cells | myocardial | Gq-coupled protein receptors

Cardiac adaptation to loading stress involves a complex process of chamber remodeling and myocyte molecular modifications. In response to increased pathological stress, myocytes enlarge and increase protein synthesis, coupled with excessive activation of multiple signaling cascades. Previous studies have revealed that Gαq-coupled receptor signaling plays a central role in this pathophysiologic process and in turn has been linked to augmented intracellular calcium signaling (1). For example, myocyte stimulation by agonists such as angiotensin II (Ang II) or endothelin-1 (ET-1) or by mechanical stress accompanying sustained hypertension leads to activation of the Ca^{2+}-calmodulin–dependent phosphatase calcineurin (Cn), which dephosphorylates the transcriptional regulator nuclear factor of activated T cells (NFAT) (2). This results in nuclear NFAT translocation where it coordinates expression of maladaptive hypertrophic genes.

The source of the triggering Ca^{2+} that leads to Cn/NFAT activation has been the subject of debate, but recent work suggests that members of the transient receptor potential canonical channel superfamily, TRPC3 and TRPC6, likely play a central role (3–5). TRPC3 and TRPC6 are highly homologous non–voltage-gated and nonselective cation channels (6, 7). They are normally expressed at very low levels in myocytes, but levels are increased in cardiac disease, such as pressure overload (3, 4, 8, 9). TRPC6 is essential for the transformation of fibroblasts to myofibroblasts and corresponding scar formation (10). Both species can be directly activated by diacylglycerol coupled to Gαq signaling, and TRPC6 is also stimulated by mechanical stretching and oxidative stress (7, 11, 12). Cardiac myocyte-targeted overexpression of either protein stimulates chamber hypertrophy and dysfunction coupled to Cn/NFAT activation in a feed-forward manner, because both channel genes also contain NFAT consensus sequences in their promoters (3, 4). To date, genetic loss-of-function studies have relied almost entirely on myocyte-targeted expression of dominant negative proteins (8) which suppresses hormone-stimulated or pressure-overload induced hypertrophy; however, because the channels can form heterotetramers (13), this approach may afford a poison peptide effect, in which a mutated channel protein interacts with other subtypes. If so, then this effect should differ from a pure gene deletion model, although this has not been reported to date.

Significance

Cardiac hypertrophy and dysfunction in response to sustained hormonal and mechanical stress are sentinel features of most forms of heart disease. Activation of non–voltage-gated transient receptor potential canonical channels TRPC3 and TRPC6 may contribute to this pathophysiology and provide a therapeutic target. Effects from combined selective inhibition have not been tested previously. Here we report the capability of highly selective TRPC3/6 inhibitors to block pathological hypertrophic signaling in several cell types, including adult cardiac myocytes. We show in vivo redundancy of each channel; individual gene deletion was not protective against sustained pressure overload, whereas combined deletion ameliorated the response. These data strongly support a role for both channels in cardiac disease and the utility of selective combined inhibition.

Author contributions: K.S., P.P.R., V.S.H., J.J.L., C.G.S., and D.A.K. designed research; K.S., P.P.R., V.S.H., D.-i.L., S.-H.J., A.A., and T.L. performed research; X.X., R.N.W., J.J.L., J.P.M., L.B., and C.G.S. contributed new reagents/analytic tools; K.S., P.P.R., V.S.H., D.-i.L., S.-H.J., A.A., T.L., R.N.W., and D.A.K. analyzed data; K.S., P.P.R., and D.A.K. wrote the paper; and D.A.K. oversaw the study and experimental design.

Conflict of interest statement: X.X, R.N.W., J.J.L., J.P.M., and C.G.S. are employees of Glaxo Smith Kline and contributed substantial resources in developing the new TRPC3/6 channel blockers.

This article is a PNAS Direct Submission.

[1]K.S., P.P.R., and V.S.H. contributed equally to this work.

[2]To whom correspondence should be addressed. E-mail: dkass@jhmi.edu.

This article contains supporting information online at www.pnas.org/lookup/suppl/doi:10.1073/pnas.1308963111/-/DCSupplemental.

MEDICAL SCIENCES

Studies using small-molecule inhibitors to examine potential benefits of TRPC3 and particularly TRPC6 blockade on heart disease have been stymied by a lack of potent selective antagonists. Inhibitors such as SKF-96365, 2-aminoethoxydiphenyl borate (14), and spider venom GsMTx-4 (15) are nonselective. Pyr3 (ethyl-1-(4-(2,3,3-trichloro-acryl- amide)phenyl)-5-(trifluoromethyl)-1H-pyrazole-4-carboxylate) has been identified as a selective TRPC3 antagonist (16, 17), although members of the 5-(trifluoro-methyl)-1H-pyrazole family to which it belongs block Ca^{2+} release-activated calcium (CRAC) channels, such as Orai channels (18, 19).

Washburn et al. (20) recently identified aniline-thiazole pharmacophore-based blockers of both TRPC3 and TRPC6 that confer nanomolar potency and selectivity. The physiological effects of these compounds have not been studied, however. Here we examined the modulation of hypertrophic stimulation in cardiac myocytes and selectivity for TRPC3 and TRPC6. We studied the differential impact of single versus combined TRPC3/TRPC6 suppression using gene deletion models. Our findings support the utility of selective TRPC3/6 antagonism in blocking cardiomyocyte hypertrophic signaling, and the benefits of targeting both TRPC species in this setting.

Results

Pharmacological Comparison of TRPC3/6 Dual Antagonists (GSK255B and GSK503A) with Pyr3. The two compounds used in this study, GSK2332255B (GSK255B) and GSK2833503A (GSK503A), are structurally similar, potent, and selective inhibitors of TRPC3/6 with ≥100-fold selectivity over other calcium-permeable channels (e.g., 10^4-fold higher IC_{50} for Cav1.2) (20). They display up to 100-fold greater potency for TRPC3 compared with Pyr3 (Table 1), and, unlike Pyr3, also inhibit TRPC6. Consistent with previous reports (19), we also found that Pyr3 blocks store-operated calcium entry (SOCE) using Jurkat cells, which have high levels of CRAC, at similar potency as it inhibits TRPC3. The same assay showed no activity against SOCE with GSK255B (Table 1).

Effect of Dual TRPC3/6 Blockade in Cultured HEK293T Cells. We first tested the efficacy of TRPC3/6 blockade in a heterologous cell system, using HEK293T cells transfected with TRPC3, TRPC6, or empty vector, along with the angiotensin type-1 receptor and an NFAT-luciferase reporter. We then stimulated the cells with Ang II with or without GSK255B. HEK293T cells normally express very low levels of TRPC3 and no TRPC6. Consistent with this, cells administered empty vector (pcDNA) and stimulated with Ang II (10 nM) exhibited NFAT activation that was unaltered by GSK255B or its inactive control (GSK383A) (Fig. 1 *A* and *B*). Cells overexpressing (>50-fold) either channel had increased basal NFAT activation that was further amplified by Ang II. This response was suppressed in a dose-dependent manner by GSK255B, but not by inactive control (Fig. 1 *A* and *B*).

To test whether GSK255B suppressed non–voltage-dependent sarcolemmal Ca^{2+} influx, we loaded nonelectrically stimulated neonatal myocytes with the Ca^{2+} sensor Fura-2/AM superfused with 0 mM Ca^{2+} and 1 μM thapsigargin, the latter to eliminate sarcoplasmic reticular Ca^{2+} sources. We then exposed the myocytes to vehicle or to 20 μM phenylephrine (PE), followed by a switch to 2 mM extracellular Ca^{2+} (Fig. 1*C*). This protocol elicited an increase in intracellular Ca^{2+} that was further augmented by PE. The stimulated response was fully prevented by coexposure to GSK255B.

TRPC6 contains two residues in the N terminus, T70 and S322, that when phosphorylated by protein kinase G (PKG) potently suppress channel conductance and corresponding NFAT activation (9, 21). Thus, we tested whether the TRPC3/6 antagonists were redundant or additive to this potent posttranslational regulation. HEK293T cells were transfected with either WT-TRPC6 or a phosphomimetic mutant form (TRPC6-SETE) in which both PKG-targeted residues were changed to glutamate. As shown in Fig. 1*D*, Ang II-stimulated NFAT-luciferase activity in cells expressing WT-TRPC6 was double that in cells expressing

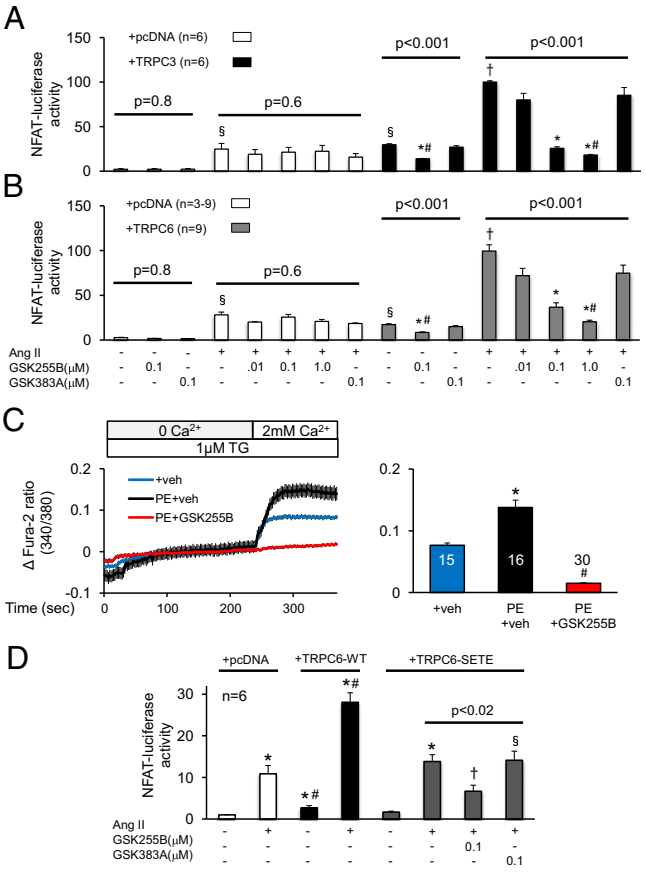

Fig. 1. Efficacy of TRPC3/6 inhibitor GSK255B on hormone-induced hypertrophic signaling in cells. NFAT activation by Ang II is blocked in a dose dependent manner by GSK255B (0.01, 0.1, and 1 μM) in HEK293T cells overexpressing TRPC3 (*A*) or TRPC6 (*B*). Cells without channel up-regulation show less Ang II-stimulated NFAT, and no response to the inhibitors, supporting selectivity. An inactive control compound (GSK383A) is also tested at 0.1 μM concentration, and shows no impact. *P* values shown are for one-way ANOVA or KW test; symbols denote results of unpaired or post hoc multiple-comparison tests: $^{\#}P < 0.05$ vs. inactive control; $^{*}P < 0.05$ and $^{\dagger}P < 0.005$ vs. vehicle control and Ang II + pcDNA; $^{\S}P < 0.005$ vs. Ang II + TRPC3 (or TRPC6) and $P < 0.005$ vs. vehicle + pcDNA. (*C*) GSK255B (10 μM) blocks calcium entry stimulated by PE (20 μM) in rat neonatal cardiac myocytes. TG, thapsigargin (1 μM). (*D*) GSK255B blocks NFAT activation by Ang II in HEK293T cells expressing a mutant TRPC6 channel with T70 and S322 mutated to glutamic acid (SETE). Data were analyzed by one-way ANOVA or the Kruskal–Wallis test in the Ang II treatment group for all three TRPC6 channel types. Post hoc testing: $^{*}P < 0.01$ vs. non–Ang II-stimulated control for pcDNA, TRPC6-WT, or TRPC6-SETE transfected cells; $^{\#}P < 0.005$ vs. corresponding response (with or without Ang II) for pcDNA or TRPC6-SETE transfected cells; $^{\dagger}P < 0.05$ vs. other groups in one-way ANOVA (horizontal line identifies groups). $^{\S}n = 3$ for this group.

Table 1. Potency of TRPC3/TRPC6 antagonists compared with Pyr3

Compound	rTRPC6, IC_{50}, μM	rTRPC3, IC_{50}, μM	CRAC, IC_{50}, μM
Pyr3 (SB-360475)	>10	0.47	0.8
GSK2332255B	0.004	0.005	>15
GSK2833503A	0.003	0.021	Not determined

TRPC6-SETE; however, this expression was still further suppressed by GSK255B but not the negative control compound, GSK383A.

Effect of Dual TRPC3/6 Inhibition in Cultured Cardiomyocytes. We next tested whether the TRPC3/6 antagonists suppress NFAT activation in both neonatal rat and adult mouse cardiac myocytes. For these and subsequent studies, we used GSK503A, which is similar to GSK255B but considered to have potentially better in vivo pharmacodynamics. Neonatal cardiomyocytes were transfected with an adenovirus encoding a luciferase-coupled reporter for regulator of Cn (Rcan-1) serving as a readout for Cn/NFAT activation. Cells stimulated with 0.1 μM ET-1 exhibited a threefold increase in Rcan-1 that was suppressed by GSK503A in a dose-dependent manner, with complete inhibition at 5–10 μM. Incubation with the corresponding negative control compound (GSK678A) did not suppress Rcan-1 luciferase activity (Fig. 2*A*). The same experiment performed with GSK255B yielded nearly identical results (Fig. S1).

Voltage-gated calcium entry is associated with hypertrophic signaling. Because the effective dose in myocytes exceeded that previously tested against Cav1.2 (20), we performed patch-clamp analysis in adult mouse myocytes using 10 μM GSK503A. As shown in Fig. 2*B*, even this high dose had no effect on the L-type calcium channel (LTCC) current-voltage (I-V) dependence.

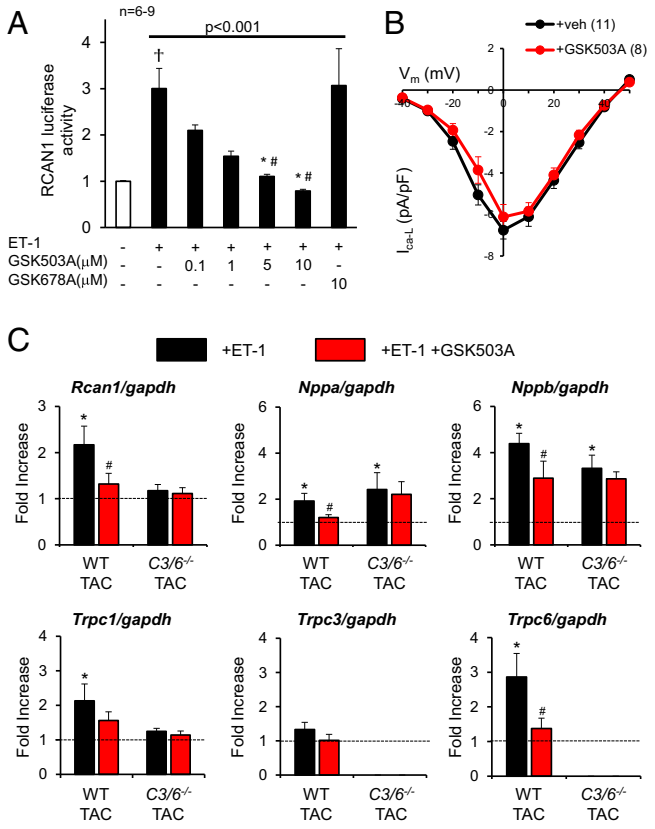

Fig. 2. Effects of TRPC3/6 inhibitor GSK503A on isolated cardiomyocytes. (*A*) GSK503A (0.1, 1, 5, and 10 μM) dose-dependently inhibits ET-1–stimulated Rcan-1 luciferase activity in rat neonatal myocytes. $^{\#}P < 0.05$ vs. inactive control (GSK678A); $^{*}P < 0.05$ vs. vehicle control. (*B*) Current-voltage (I-V) relationship for L-type Ca^{2+} current ($I\text{-}V_{Ca\text{-}L}$) in adult mouse cardiomyocytes treated with GSK503A (10 μM). (*C*) Gene expression of hypertrophy-related genes and TRPC channels in adult myocytes exposed to 24 h of ET-1 with or without coinhibition of TRPC3/6 (GSK503A, 10 μM). $n = 6$–9 for each condition. *Rcan1*: $^{*}P < 0.03$ vs. control, $^{\#}P = 0.011$ vs. ET-1; *Nppa*: $^{*}P < 0.01$ vs. control, $^{\#}P < 0.03$ vs. ET-1; *Nppb*: $^{*}P < 0.001$ vs. control, $^{\#}P < 0.03$ vs. ET-1; *Trpc1*: $^{*}P = 0.06$ vs. control; *Trpc6*: $^{*}P = 0.01$ vs. control, $^{\#}P < 0.05$ vs. ET-1.

For evaluation of the effect of GSK503A in adult myocytes, hearts from C57BL/6J mice were first subjected to pressure overload (i.e., aortic constriction) to augment basal channel expression (9). Myocytes were then isolated and were subjected to 24-h stimulation with 0.1 μM ET-1 with or without 10 μM GSK503A. Fetal gene markers of pathological hypertrophy (*Nppa* and *Nppb*), as well as *Rcan1*, *Trpc6*, and *Trpc1*, all increased with ET-1 stimulation (Fig. 2*C*). The increase in TRPC channel expression is consistent with a feed-forward activation coupled to Ca^{2+}-stimulated NFAT activity (3, 22). Coincubation with GSK503A blunted these changes. When the same experiment was performed in cells genetically lacking both TRPC3/6, the response was attenuated compared with WT cells and was unchanged by the addition of GSK503A. *Trpc1* expression also increased with ET-1 in WT cells, and this response was blunted by GSK503A as well. Both the rise and drug-induced decline in *Trpc1* expression were not observed in double KO (dKO) cells exposed to ET-1, indicating that this is an indirect effect of the suppression of TRPC3/6 rather than an off-target influence of GSK503A.

TRPC3/6 Combined Mice, But Not Single-Channel KO Mice, Are Protected Against Pressure Overload-Induced Pathological Remodeling. The library screen for TRPC3 or TRPC6 antagonists identified compounds generally sensitive to both (20). Selective targeting previously has been achieved either by dominant negative expression (8) or with Pyr3, which inhibits TRPC3 (16), both of which produce antihypertrophic effects. This leaves open the question of whether similar efficacy occurs when a single species is genetically deleted. To test this, we subjected mice lacking TRPC3, TRPC6, or both to 3 wk of pressure overload by transverse aortic constriction (TAC). Selective gene deletion is shown in Fig. S2. Resting left ventricular (LV) mass and fractional shortening were similar between each KO group and its respective littermate controls (Fig. 3 *A*–*C*). The absolute response to TAC in each control group varied slightly among genotypes ($P = 0.03$, one-way ANOVA), likely reflecting differences in C57BL/6J/sv129 background. In *TRPC3*$^{-/-}$ and *TRPC6*$^{-/-}$ mice, TAC induced similar hypertrophy and reduced fractional shortening as observed in the TAC control mice. The slightly worse-appearing function in *TRPC3*$^{-/-}$ (nonsignificant) may be related in part to persistent TRPC6 expression (Fig. S2). In contrast, mice lacking both genes displayed a blunted response to TAC (Fig. 3*C*). Whereas the dKO mice displayed normal fractional shortening at 3 wk, this declined after 6–7 wk to levels midway between those of sham and TAC controls, matching levels of suppressed hypertrophy (Fig. S3).

The disparate hypertrophic responses in the three models were further confirmed by postmortem analysis of heart weight/tibia length (Fig. 4*A*) and myocyte cross-sectional area (Fig. 4*B* and Fig. S4), and were correlated with expression of heart failure markers. In TAC *TRPC 3*$^{-/-}$ and *TRPC6*$^{-/-}$ mice, *Nppa* and *Nppb* expression remained elevated as in the littermate controls, but were diminished in TRPC3/6 dKO mice exposed to TAC (Fig. 4*C*). We further examined whether alternative TRPC channels were regulated in each model before and after TAC. *Trpc1* expression was similar at baseline among the models and changed only minimally after TAC (Fig. S2).

Assessment of GSK503A in an in Vivo Rat Model of Pressure Overload. We found that testing the efficacy of either GSK255B or GSK503A in vivo was impossible in mice, whose extremely fast metabolism precluded us from obtaining stable effective plasma concentrations. Testing in rats seemed more plausible, but unfortunately, this model proved inadequate as well. In the rat trial, adult rats underwent ascending aortic constriction (AAC) at 1 wk

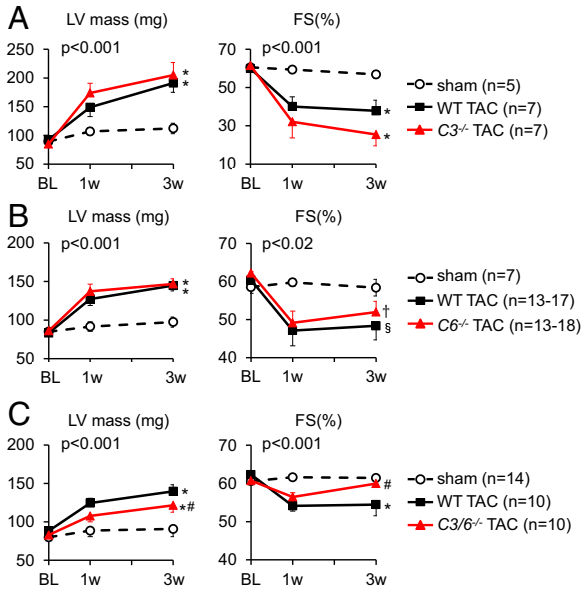

Fig. 3. Echocardiographic analyses of LV mass and fractional shortening in mice selectively lacking (*A*) Trpc3 (C3-/-), (*B*) Trpc6 ($C6^{-/-}$), or (*C*) both genes and their respective littermate controls (WT) each subjected to TAC. *P* values denote (group) × (time) interaction based on ANCOVA; symbols identify interaction terms for pairwise covariance analysis versus sham control (*$P < 0.001$; †$P < 0.02$; §$P < 0.01$) or WT-TAC (#$P < 0.02$). Sham control data combine both littermates and KOs for each group, because there was no significant difference between them.

after initiation of treatment on a maximal dose of GSK503A (300 mg/kg/wk s.c.) or vehicle control, and were then followed for 7 wk. Total plasma concentration of GSK503A ranged from 200 to 600 ng/mL (0.5–1.5 μM), yielding a protein-free plasma concentration of <0.05 μM. Based on our neonatal rat cardiac ventricular myocyte assay (Fig. 2*A*), we expected this level to be insufficient to suppress myocyte hypertrophy, and indeed chronic treatment did not alter LV mass, fractional shortening, or maximal rate of pressure rise, dP/dt_{max} (Fig. S5*A*). We did observe significant fibrosis in vehicle-treated hearts that was not present with GSK503A treatment ($P < 0.02$, one-way ANOVA). AAC increased expression of *Trpc3*, *Trpc6*, *Rcan1*, and gene markers of pathological hypertrophy (Fig. S5*B*). Treatment prevented the rise in TRPC3 and attenuated the rise in TRPC6 (although the latter remained fourfold above baseline), but did not significantly blunt the other biomarkers.

Discussion

This study confirms the physiological efficacy and selectivity of two recently developed TRPC3/TRPC6 antagonists that lack activity against voltage-gated Ca^{2+} and SOCE channels and blunt Gαq agonist-stimulated hypertrophy in neonatal and adult cardiac myocytes. Although the in vivo experiments in rodents were limited by inadequate pharmacokinetics, further testing showed that gene deletion of TRPC3 or TRPC6 alone is not protective against pressure overload in vivo, whereas their combined deletion is protective.

Despite growing evidence supporting its role in pathological heart disease, therapeutic TRPC3 or TRPC6 inhibition has been limited by a lack of selective small-molecule inhibitors. BTP2 (*N*-[4-(3,5-bis(trifluoromethyl)-1H-pyrazol-1-yl)phenyl]-4-methyl-1,2,3-thiadiazole -5-carboxamide) targets multiple TRPC and CRAC channels (23), whereas the inositol triphosphate receptor blocker SKF96365 targets both TRPC and T-type Ca^{2+} channels (24). Pyr3, the first reported selective TRPC3 blocker, suppresses hypertrophic signaling in pressure-overloaded hearts in vivo (16); however, its impact is relatively mild, with a reported IC_{50} against TRPC3 of 0.7 μM (vs. 21 nM for GSK503A), and it is inactive against TRPC6. Pyr3 also inhibits SOCE due to Orai-1, at concentrations close to that for TRPC3 (our data and ref. 19), raising concerns regarding its selectivity. Selective TRPC6 inhibitors were recently reported by Urban et al. (25) using the Chembionet library; however, their IC_{50} for channel blockade ranged from 3 to 15 μM, and no assessment of hypertrophic modulation was reported.

Given this background, GSK255B and GSK503A (20) represent major advances in both sensitivity and selectivity against TRPC3 and TRPC6, with activity in the nM range for cell calcium entry. In HEK cells, 0.1 μM was efficient to markedly reduce NFAT activity assayed by a luciferase reporter, and although higher doses were required in neonatal and adult cardiac myocytes, the selectivity of the blockers persisted, as confirmed both by the absence of effects in cells lacking both channels and the lack of effect on LTCC I-V dependence. We observed a small but significant rise in TRPC1 expression in adult myocytes exposed to ET-1 that was also suppressed by GSK503A. However, this likely was not an off-target effect, given that gene TRPC1 expression was unchanged from baseline in ET-1–treated myocytes lacking only TRPC3/6, and GSK503A had no further influence in this setting.

An important question relevant to the development of small-molecule TRPC3 and/or TRPC6 inhibitors is whether blockade of either channel alone is sufficient to ameliorate cardiac pathology. Both channels are highly homologous and share properties of G-coupled receptor activation, stimulation of Cn/NFAT, and up-regulation via an NFAT-consensus sequence in their respective promoters (6). TRPC3 and TRPC6 are known to heterotetramerize based on immunoprecipitation and fluorescence resonance energy transfer studies (26). Genetic models involving expression of dominant negative proteins (8) may induce a promiscuous effect on the other channel and other TRPC channels; for instance, TRPC1 also multimerizes with TRPC3 (27). The present study supports this hypothesis, because neither single gene deletion model ameliorated hypertrophy/dysfunction with TAC, whereas the dKO model was more effective.

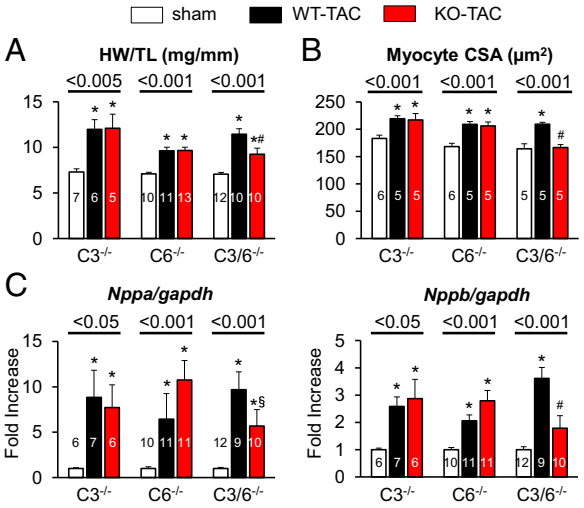

Fig. 4. Analyses of morphometric and molecular parameters of hypertrophy in mice selectively lacking *Trpc3*, *Trpc6*, or both genes and then subjected to TAC. (*A*) Heart weight/tibia length (at 6–7 wk for dKO and controls and 3 wk for other models). (*B*) Myocyte cross-sectional area assessed by wheat germ agglutinin staining at the terminal study for each model. *P* values for one-way ANOVA for each genotype, post hoc test results: *$P < 0.05$ vs. sham; #$P < 0.05$ vs. WT-TAC. (*C*) Response of hypertrophy-related fetal genes (*Nppa* and *Nppb*) for each model. *$P < 0.05$ vs. sham; #$P < 0.05$ vs. WT-TAC; §$P = 0.07$ vs. WT-TAC.

From the perspective of drug development, however, it remains possible that agents targeting one channel subtype will similarly affect the other subtype in a heterotetramer. This could explain the efficacy of Pyr3 despite its blockage of only TRPC3. Whether this or a dual-channel blocker is the optimal strategy remains unclear because of the uncertain stoichiometry of these channel subunits in vivo, particularly when one species is more highly up-regulated, as often the case for TRPC6. In this regard, our present in vivo rat study found that even with suppression of TRPC3 back to resting levels, persistent marked elevation of TRPC6 despite GSK503A administration correlated with the lack of an altered hypertrophy phenotype.

The magnitude of Ca^{2+} entry via TRPC3 or TRPC6 is considered quite small relative to that from voltage-gated channels, raising the suspicion that some interaction between these species is essential for maladaptive hypertrophy signaling (28). Others have shown that TRPC6-stimulated NFAT activity is not inhibited by the LTCC blocker nifedipine, however (9). Klaiber et al. (29) reported that Ca^{2+} entry in response to Ang II was depressed in myocytes lacking both TRPC3 and TRPC6, whereas entry in response to isoproterenol was unchanged despite direct engagement of LTCC channels by the latter. Our present data further support separation of these calcium pools, because the TRPC3/6 antagonists exert no demonstrable inhibitory activity against LTCC, yet suppress hypertrophy signaling only in cells expressing both TRPC species.

Our study has several limitations. The gene KO models were global, so the relative contribution of myocytes versus fibroblasts or smooth muscle cells cannot be discerned. Previous myocyte-targeted dominant negative approaches (8) and our present in vitro data support relevance in myocytes, however. Because small-molecule inhibitors likely influence multiple cell types as well, these global KO data are relevant. Moreover, the models displayed a less-marked hypertrophic response even in littermate controls, as seen in pure C57BL/6J mice, which may explain the lack of rise in TRPC3 expression and the more modest rise in TRPC6 compared with some previous data (9, 16). Finally, despite the considerable effort in rats, translation of the new TRPC3/6 antagonists in vivo must await further pharmacokinetic modifications so that adequate plasma concentrations can be achieved. Nonetheless, the compounds presented here represent a class that obviates many of the ambiguities associated with existing inhibitors and will enhance basic studies of these channels and their role to a growing range of disease conditions.

Materials and Methods

Pharmaceuticals. Selective dual TRPC3/TRPC6 small-molecule inhibitors GSK2332255B (GSK255B, example 17) and GSK2833503A (GSK503A, example 19) and corresponding inactive controls [GSK2346383A (GSK383A) and GSK2402678A (GSK678A)] were studied (20). GSK255B has an IC_{50} = 5 nM for TRPC3 and 4 nM for TRPC6, whereas GSK503A has an IC_{50} = 21 nM for TRPC3 and 3 nM for TRPC6, as determined by patch- clamping in HEK cells expressing both channels (*SI Materials and Methods*). Both inactive controls had an IC_{50} > 25 μM for both TRPC3 and TRPC6. These compounds were also tested against voltage-gated calcium channels (CaV1.2, IC_{50} = 0 μM), hERG (IC_{50} > 50 μM), and NaV1.5 (IC_{50} > 3.3 μM). All compounds were first dissolved in 100% DMSO and then diluted 1:1,000 in culture media. Ang II and ET-1 (Sigma-Aldrich) were diluted in nuclease-free double-distilled H_2O. These studies initially used GSK255B, but once GSK503A was identified and appeared to be slightly more potent with potentially more favorable in vivo pharmacokinetics, this compound was substituted. Both compounds were tested in the same neonatal myocyte assay.

Plasmids. We obtained pcDNA3-human TRPC6-YFP from Craig Montell (Molecular, Cellular, and Developmental Biology, University of California Santa Barbara, Santa Barbara, CA) (30), pcDNA3-human TRPC3 from Jeffery Molkentin (Howard Hughes Medical Institute, Cincinnati Childrens Hospital Medical Center, Cincinnati), and pcDNA3-mouse angiotensin II type 1 receptor (AT1R) from Akiyoshi Fukamizu (Life Science Center, Tsukuba Advanced Research Alliance, University of Tsukuba, Tsukuba, Ibaraki, Japan) (31). pGL4.30-NFAT-RE firefly luciferase vector (NFAT-luc) with an NFAT response element driving the transcription of firefly luciferase, pGL4.75-CMV *Renilla* luciferase vector (CMV-Rluc), and pGL4.74-TK (thymidine kinase) *Renilla* luciferase (TK-Rluc) vector were purchased from Promega. A TRPC6-phosphomimetic mutant (S322E and T70E) was generated by PCR-based site mutagenesis (QuikChange; Stratagene) using pcDNA3-human TRPC6-YFP as the template, as described previously (9). pcDNA3 served as an empty vector control for all transfection protocols. pGL3-RCAN1-firefly luciferase vector, in which RCAN1 intron 3 containing 15 NFAT-binding sites was inserted upstream of the luciferase reporter gene, was generated by Beverly Rothermel and provided by Eric Olson (Department of Molecular Biology, University of Texas Southwestern, Dallas) (32).

TRPC3/6 Gene Deletion Mice. TRPC3 KO (*TRPC3*$^{-/-}$) and TRPC6 KO (*TRPC6*$^{-/-}$) mice were previously generated as described (33, 34). Each individual KO mouse model was backcrossed for at least five generations into a C57BL/6J background, and their cross yielded the combined TRPC3/TRPC6 dKO (*TRPC3/6*$^{-/-}$) mouse. Age-matched KO and WT littermate controls were used for all studies. All experiments were conducted in accordance with National Institutes of Health Guidelines for the Care and Use of Animals and were reviewed by the Institutional Animal Care and Use Committee at the institution where the work was performed.

HEK293T Cell Experiments. HEK293T cells were cultured to 50% confluence and then transfected with plasmid containing AT1R, NFAT-luc, and CMV-luc (internal control) as described previously (9). HEK293T cells do not express TRPC6 and express TRPC3 only at very low levels. For our studies, cells were transfected with WT-TRPC3, WT-TRPC6, or empty vector pcDNA to augment signaling to channel stimulation by a Gαq receptor-coupled agonist. After transfection, cultures were maintained in serum-free medium for 24 h. Cultures were then treated with Ang II with or without a TRPC3/6 inhibitor, vehicle, or inactive control for 4 h, then harvested using the Dual-Luciferase Reporter Assay System (Promega), following the manufacturer's protocol.

Isolated Ventricular Myocyte Studies. Neonatal rat cardiac ventricular myocytes were isolated from 1- to 3-d-old Sprague–Dawley rats as described previously (35). Cultures were maintained in 10% FBS containing culture medium for 36 h after isolation. Cells were transfected with RCAN1-luc and TK-luc (as an internal control) using Xfect transfection reagent (Clontech) according to the manufacturer's protocol. After transfection, cells were maintained in serum-free medium for 24 h, then exposed to ET-1 with or without TRPC3/6 inhibitor, vehicle, or inactive control for 24 h. Cells were harvested with cell lysis buffer (Promega), and luciferase activity was measured with a GloMax 96 microplate luminometer (Promega) using the Dual-Luciferase Report Assay System (Promega).

For functional studies of cytosolic Ca^{2+}, cells were loaded with 1 μM Fura-2/AM (Molecular Probes) for 20 min at room temperature in serum-free medium or in Tyrode's solution containing 10 mM Hepes, 140 mM NaCl, 5 mM KCl, 1 mM $MgCl_2$, 1 mM $CaCl_2$, and 5.5 mM glucose (pH 7.4). After incubation, cells were bathed in Ca^{2+}-free Tyrode's solution and then incubated with 1 μM thapsigargin and 20 μM PE. The solution was then switched to 2 mM Ca^{2+}-Tyrode's solution with thapsigargin to assess Ca^{2+} influx in the presence of PE with or without the TRPC3/6 inhibitor (GSK255B, 10 μM). Cytosolic Ca^{2+} was monitored with an Olympus IX81 inverted fluorescence microscope and Slidebook software, using excitation wavelengths of 340 and 380 nm to detect Fura-2/AM fluorescence emission at 510 nm.

Studies were also performed in primary ventricular myocytes isolated from adult mice from dKO and littermate controls following the methodology of O'Connell et al. with minor modifications (9, 36). To enhance expression of the channels, which is low under normal conditions, hearts were subjected to 1 wk of pressure overload (i.e., TAC) (9). After euthanasia, the mouse heart was promptly removed from the chest, and the aorta was retroperfused at 37 °C for 3 min with a Ca^{2+}-free bicarbonate-based isolation buffer. Enzymatic digestion was initiated by adding 0.9 mg/mL collagenase type 2 (Worthington) and 0.05 mg/mL protease type XIV (Sigma-Aldrich) to the perfusion solution for 6–7 min. Dispersed myocytes were incubated in buffer with increasing concentrations of Ca^{2+}, finally achieving a concentration of 1.2 mM Ca^{2+} as in MEM culture media (Sigma-Aldrich) containing insulin-transferrin-selenium and penicillin-streptomycin (Gibco).

Cells were seeded at 25,000 rod-shaped myocytes/mL on six-well laminin-coated plates. The myosin ATPase inhibitor 2,3-butanedione monoxime (10 mM) was added to the perfusion buffer and culture medium to provide myocyte cytoprotection. At 1 h after incubation at 37 °C in 5% CO_2, the culture medium was replaced to remove unattached cells, and cells were stimulated with ET-1 (0.1 μM) with or without concomitant TRPC3/6 blockade (GSK503A,

10 μM). Cells were harvested 24 h later and analyzed by quantitative PCR (qPCR) to assess expression of hypertrophic signaling genes.

In Vivo Pressure Overload Studies. TAC was performed in 10- to 16-wk-old TRPC3 KO and TRPC6 KO and dKO mice and corresponding littermate controls as described previously (9). Sham-operated mice underwent the same surgery without aortic constriction. Conscious mice were assessed by serial echocardiography (Acuson Sequoia C256, 13-MHz transducer; Siemens), and chamber dimensions and LV mass were measured (heart rate >600 min^{-1}). The analysis was blinded to genotype. All protocols were approved by The Johns Hopkins University Animal Care and Use Committee.

For rat studies, Wistar rat weanlings (~50 g, 3 wk) were pretreated with vehicle (corn oil 10 mL/kg once weekly s.c.) or GSK503A (300 mg/kg) for 7 d. The rats were then anesthetized with isoflurane (Abbot Scandinavia) and ventilated (UB 7025; Hugo Sachs Elektronik/Harvard Apparatus). The ascending aorta was accessed and constricted as described previously (37). Sham animals underwent the same procedure without banding. Drug plasma concentrations were measured at 1, 4, and 8 wk after the start of treatment. All experiments were performed in accordance with the Guide for the Care and Use of Laboratory Animals published by the National Institutes of Health (Publication 85-23, revised 1985) and were approved by the Danish Animal Experiments Inspectorate (2012-15-2934-00071).

Rat echocardiography was performed by a trained and blinded operator using a Vivid 7 echocardiography system (GE Healthcare) with an 11-MHz transducer on lightly anesthetized rats. LV pressures were assessed transapically using a 1.4F pressure catheter (Millar Instruments).

Patch-Clamp Studies, Histology, and Gene Expression by qPCR. Detailed information on patch-clamp studies, histology, and qPCR assays is provided in *SI Materials and Methods*.

Statistical Analysis. Statistical analyses were performed with one-way or two-way ANOVA for normally distributed data with equal variance among groups and with the Kruskal–Wallis test for other data. Post hoc analysis was performed using the Tukey–Kramer or Mann–Whitney *U* test, as appropriate, along with the Fisher least squares estimate test. Analyses were performed using SigmaStat version 13 and Systat version 10 software.

ACKNOWLEDGMENTS. We thank Djahida Bedja (Johns Hopkins University) for technical assistance. This work was supported by a grant from GlaxoSmithKline. Additional funding was provided by an American Heart Association Mid-Atlantic Fellowship Grant (to K.S. and D.-i.L.), a Research Fellowship from the Sarnoff Cardiovascular Research Foundation (to V.S.H.), a Max Kade Fellowship from the Austrian Academy of Sciences (to P.P.R.), the National Research Foundation of Korea (Grant 2011-0013171, to S.-H.J.), the Danish Council for Independent Research (Grant 11-108410, to A.A.), the Intramural Research Program of the National Institutes of Health (Project Z01-ES-101864, to L.B.), National Institutes of Health Grants HL089297 and HL059408, Muscular Dystrophy Association Grant 186454, an Abraham and Virginia Weiss Professorship, and the Peter Belfer Endowment (D.A.K.).

1. D'Angelo DD, et al. (1997) Transgenic Gαq overexpression induces cardiac contractile failure in mice. *Proc Natl Acad Sci USA* 94(15):8121–8126.
2. Wilkins BJ, et al. (2004) Calcineurin/NFAT coupling participates in pathological, but not physiological, cardiac hypertrophy. *Circ Res* 94(1):110–118.
3. Kuwahara K, et al. (2006) TRPC6 fulfills a calcineurin signaling circuit during pathologic cardiac remodeling. *J Clin Invest* 116(12):3114–3126.
4. Nakayama H, Wilkin BJ, Bodi I, Molkentin JD (2006) Calcineurin-dependent cardiomyopathy is activated by TRPC in the adult mouse heart. *FASEB J* 20(10):1660–1670.
5. Onohara N, et al. (2006) TRPC3 and TRPC6 are essential for angiotensin II-induced cardiac hypertrophy. *EMBO J* 25(22):5305–5316.
6. Eder P, Molkentin JD (2011) TRPC channels as effectors of cardiac hypertrophy. *Circ Res* 108(2):265–272.
7. Patel A, et al. (2010) Canonical TRP channels and mechanotransduction: From physiology to disease states. *Pflugers Arch* 460(3):571–581.
8. Wu X, Eder P, Chang B, Molkentin JD (2010) TRPC channels are necessary mediators of pathologic cardiac hypertrophy. *Proc Natl Acad Sci USA* 107(15):7000–7005.
9. Koitabashi N, et al. (2010) Cyclic GMP/PKG-dependent inhibition of TRPC6 channel activity and expression negatively regulates cardiomyocyte NFAT activation: Novel mechanism of cardiac stress modulation by PDE5 inhibition. *J Mol Cell Cardiol* 48(4):713–724.
10. Davis J, Burr AR, Davis GF, Birnbaumer L, Molkentin JD (2012) A TRPC6-dependent pathway for myofibroblast transdifferentiation and wound healing in vivo. *Dev Cell* 23(4):705–715.
11. Spassova MA, Hewavitharana T, Xu W, Soboloff J, Gill DL (2006) A common mechanism underlies stretch activation and receptor activation of TRPC6 channels. *Proc Natl Acad Sci USA* 103(44):16586–16591.
12. Ding Y, et al. (2011) Reactive oxygen species-mediated TRPC6 protein activation in vascular myocytes, a mechanism for vasoconstrictor-regulated vascular tone. *J Biol Chem* 286(36):31799–31809.
13. Lepage PK, et al. (2006) Identification of two domains involved in the assembly of transient receptor potential canonical channels. *J Biol Chem* 281(41):30356–30364.
14. Harteneck C, Gollasch M (2011) Pharmacological modulation of diacylglycerol-sensitive TRPC3/6/7 channels. *Curr Pharm Biotechnol* 12(1):35–41.
15. Suchyna TM, et al. (2000) Identification of a peptide toxin from *Grammostola spatulata* spider venom that blocks cation-selective stretch-activated channels. *J Gen Physiol* 115(5):583–598.
16. Kiyonaka S, et al. (2009) Selective and direct inhibition of TRPC3 channels underlies biological activities of a pyrazole compound. *Proc Natl Acad Sci USA* 106(13):5400–5405.
17. Kim MS, et al. (2011) Genetic and pharmacologic inhibition of the Ca^{2+} influx channel TRPC3 protects secretory epithelia from Ca^{2+}-dependent toxicity. *Gastroenterology* 140(7):2107–2115.
18. Touchberry CD, et al. (2011) Store-operated calcium entry is present in HL-1 cardiomyocytes and contributes to resting calcium. *Biochem Biophys Res Commun* 416(1-2):45–50.
19. Schleifer H, et al. (2012) Novel pyrazole compounds for pharmacological discrimination between receptor-operated and store-operated Ca(2+) entry pathways. *Br J Pharmacol* 167(8):1712–1722.
20. Washburn DG, et al. (2013) The discovery of potent blockers of the canonical transient receptor channels, TRPC3 and TRPC6, based on an anilino-thiazole pharmacophore. *Bioorg Med Chem Lett* 23(17):4979–4984.
21. Kinoshita H, et al. (2010) Inhibition of TRPC6 channel activity contributes to the antihypertrophic effects of natriuretic peptides-guanylyl cyclase-A signaling in the heart. *Circ Res* 106(12):1849–1860.
22. Ohba T, et al. (2007) Upregulation of TRPC1 in the development of cardiac hypertrophy. *J Mol Cell Cardiol* 42(3):498–507.
23. Zitt C, et al. (2004) Potent inhibition of Ca^{2+} release-activated Ca^{2+} channels and T-lymphocyte activation by the pyrazole derivative BTP2. *J Biol Chem* 279(13):12427–12437.
24. Singh A, Hildebrand ME, Garcia E, Snutch TP (2010) The transient receptor potential channel antagonist SKF96365 is a potent blocker of low-voltage–activated T-type calcium channels. *Br J Pharmacol* 160(6):1464–1475.
25. Urban N, Hill K, Wang L, Kuebler WM, Schaefer M (2012) Novel pharmacological TRPC inhibitors block hypoxia-induced vasoconstriction. *Cell Calcium* 51(2):194–206.
26. Amiri H, Schultz G, Schaefer M (2003) FRET-based analysis of TRPC subunit stoichiometry. *Cell Calcium* 33(5-6):463–470.
27. Chen J, Crossland RF, Noorani MM, Marrelli SP (2009) Inhibition of TRPC1/TRPC3 by PKG contributes to NO-mediated vasorelaxation. *Am J Physiol Heart Circ Physiol* 297(1):H417–H424.
28. Gao H, et al. (2012) Ca(2+) influx through L-type Ca(2+) channels and transient receptor potential channels activates pathological hypertrophy signaling. *J Mol Cell Cardiol* 53(5):657–667.
29. Klaiber M, et al. (2010) Novel insights into the mechanisms mediating the local antihypertrophic effects of cardiac atrial natriuretic peptide: Role of cGMP-dependent protein kinase and RGS2. *Basic Res Cardiol* 105(5):583–595.
30. Kwon Y, Hofmann T, Montell C (2007) Integration of phosphoinositide- and calmodulin-mediated regulation of TRPC6. *Mol Cell* 25(4):491–503.
31. Koitabashi N, et al. (2005) Carvedilol effectively blocks oxidative stress-mediated downregulation of sarcoplasmic reticulum Ca^{2+}-ATPase 2 gene transcription through modification of Sp1 binding. *Biochem Biophys Res Commun* 328(1):116–124.
32. Yang J, et al. (2000) Independent signals control expression of the calcineurin inhibitory proteins MCIP1 and MCIP2 in striated muscles. *Circ Res* 87(12):E61–E68.
33. Hartmann J, et al. (2008) TRPC3 channels are required for synaptic transmission and motor coordination. *Neuron* 59(3):392–398.
34. Dietrich A, et al. (2005) Increased vascular smooth muscle contractility in TRPC6$^{-/-}$ mice. *Mol Cell Biol* 25(16):6980–6989.
35. Takimoto E, et al. (2005) Chronic inhibition of cyclic GMP phosphodiesterase 5A prevents and reverses cardiac hypertrophy. *Nat Med* 11(2):214–222.
36. O'Connell TD, Rodrigo MC, Simpson PC (2007) Isolation and culture of adult mouse cardiac myocytes. *Methods Mol Biol* 357:271–296.
37. Weinberg EO, et al. (1994) Angiotensin-converting enzyme inhibition prolongs survival and modifies the transition to heart failure in rats with pressure overload hypertrophy due to ascending aortic stenosis. *Circulation* 90(3):1410–1422.

Supporting Information

Seo et al. 10.1073/pnas.1308963111

SI Materials and Methods

Patch-Clamp Studies. Intracellular AlF_4^- was used to activate recombinant transient receptor potential canonical channel type 3 or type 6 (rTRPC3, rTRPC6) current in transduced HEK293 cells (1). HEK293 cells were cultured to 50–70% confluence and transduced with BacMam virus expressing the rTRPC3 or rTRPC6 gene (8–12% vol/vol) for 48 h. The transduced cells were trypsinized and stored in Dulbecco's Modified Eagle Medium DMEM/F-12 + 10% FBS at room temperature for patch-clamp experiments within 5 h. Cells were perfused with an external solution (~3 mL/min) at room temperature (22 °C). The electrodes, made from glass capillary tubes, had a resistance of 2–4 MΩ when filled with internal solution containing AlF_4^- [110 mM CsF, 20 mM CsCl, 10 mM Hepes, 10 mM EGTA, and 10 mM NaF; pH 7.2), plus 15 μM $AlCl_3$]. An Axopatch 200B amplifier and pCLAMP 8 software (Molecular Devices) were used for data acquisition and analysis.

The seal between the cell membrane and electrode was created in the external solution containing 140 mM NaCl, 4 mM KCl, 1 mM $MgCl_2$, 0.2 mM $CaCl_2$, 10 mM glucose, and 10 mM Hepes (pH 7.4). Once the whole-cell configuration was established, the external solution was switched to the EGTA-containing solution (140 mM NaCl, 4 mM KCl, 1 mM $MgCl_2$, 2 mM Na_4EGTA, 10 mM glucose, and 10 mM Hepes; pH 7.4), to minimize desensitization of the TRPC current. Cell membrane capacitance was canceled electronically, and the series resistance was compensated by approximately 70%.

To record TRPC current, a ramp voltage protocol was applied every 10 s for the suration of the experiment. The ramp protocol stepped from a holding voltage of −60 mV to −80 mV for 40 ms and then depolarized to +80 mV in 400 ms, then stepped back to holding voltage after 40 ms at +80 mV. rTRPC3 or rTRPC6 current gradually increased as the cell was dialyzed with the internal solution containing AlF_4^-. For a large portion of cells, we were able to record a relatively stable rTRPC3 or rTRPC6 current.

Once the control current stabilized, the recording chamber was perfused with the EGTA external solution containing a testing compound. At each drug concentration, 2~3 min was allowed for the drug effect to reach steady state. At the end of the experiment, a positive control compound (GSK417651A) was applied to the cell to completely block the rTRPC3 or rTRPC6 current. Zero current (background) level was set at the end of GSK417651A perfusion. The rTRPC3 or rTRPC6 current amplitude was measured as the average current at +80 mV.

We plotted the time course of current for the whole experiment: % inhibition = $100 \times (1 - I_D/I_C)$, where I_D is the current amplitude measured at the end of a particular drug concentration perfusion and I_C is the control current amplitude measured before drug application. We calculated the average % inhibition at each drug concentration first. The averaged data were fit using the four-parameter logistic equation model and Origin 7.0 software to calculate IC_{50}.

We measured L-type calcium channel current-voltage relationships by whole-cell patch-clamp studies as described previously (2). In brief, myocytes were loaded into a heated chamber (37 °C) on the stage of a fluorescence microscope (Nikon Eclipse TE300) and superfused with Cs-Tyrode's solution containing 130 mM NaCl, 5 mM CsCl, 2 mM $MgCl_2$, 10 mM Na-Hepes, 2 mM $CaCl_2$, and 10 mM glucose (pH 7.4). Myocytes were whole-cell patch-clamped with 2–4 MΩ pipettes and equilibrated with a pipette solution containing 110 mM CsCl, 0.5 mM $MgCl_2$, 10 mM Hepes, 5 mM Mg-ATP, 5 mM 1,2-bis(o-aminophenoxy) ethane-N,N,N′,N′-tetraacetic acid, and 20 mM tetraethylammonium (pH 7.25). Then 10 μM GSK503A was added to the Cs-Tyrode's solution. After achievement of whole-cell conformation, cells were voltage-clamped at a holding potential of −80 mV. L-type Ca^{2+} current ($I_{Ca\text{-}L}$) was recorded by applying a depolarizing pulse of 0 mV or a series of pulses ranging from −40 to +50 mV in 10-mV steps for 300 ms after a 200-ms prepulse to −40 mV.

CRAC Activity Assay. Calcium release activated channel activity was determined using a Fluo4 fluorescence assay in Jurkat E6-1 cells stimulated with CaCl in the presence of thapsigargin (500 nM) as described previously (1).

Histology. For wheat germ agglutinin staining of mouse heart sections, myocardium was fixed with 4% paraformaldehyde, paraffin-embedded, sectioned into 4-μm slices, deparaffinized, rehydrated, and subjected to citrate-based head-mediated antigen retrieval. Slides were incubated with 5 μg/mL Alexa Fluor 647-conjugated wheat germ agglutinin (Invitrogen) overnight at 4 °C and mounted using Prolong Gold mounting medium (Invitrogen). Image acquisition was performed on an EVOS epifluorescence microscope (Life Technologies). Myocyte cross-sectional area was measured blinded to the treatment group and genotype using an automated algorithm with Image J 1.47i software, analyzing 1,040 ± 70 cells from 6–16 areas per mouse heart.

Rat left ventricles were formalin-fixed, paraffin-embedded, and sectioned following routine procedures, then stained with Sirius red to visualize fibrosis in polarized light. Digital color images of the left ventricle (ColorViewII; Soft Imaging System) were captured and analyzed using ImageJ software after conversion to an 8-bit grayscale and manual thresholding. The mean area of fibrosis was calculated by a blinded investigator as the average percentage of images without large vessels, epicardium, or pericardium.

Gene Expression by PCR. Quantitative PCR was used to assess fetal and hypertrophic gene expression and TRPC1, TRPC3, or TRPC6 expression in cells and myocardial tissue. RNA was extracted with TRIzol (Invitrogen), and cDNA was synthesized by TaqMan reverse-transcription reagents following the manufacturer's recommended protocol (Applied Biosystems). Quantitative real-time PCR was performed with the 7900HT Sequence Detection System (Applied Biosystems) with sample duplicates. TaqMan primers and probes for rat and mouse were obtained from Applied Biosystems. Gene expression was calculated using the ΔΔCt method, and normalized to GAPDH expression.

1. Kraft R (2007) The Na^+/Ca^{2+} exchange inhibitor KB-R7943 potently blocks TRPC channels. *Biochem Biophys Res Commun* 361(1):230–236.

2. Ganesan AN, Maack C, Johns DC, Sidor A, O'Rourke B (2006) Beta-adrenergic stimulation of L-type Ca^{2+} channels in cardiac myocytes requires the distal carboxyl terminus of alpha1C but not serine 1928. *Circ Res* 98(2):e11–e18.

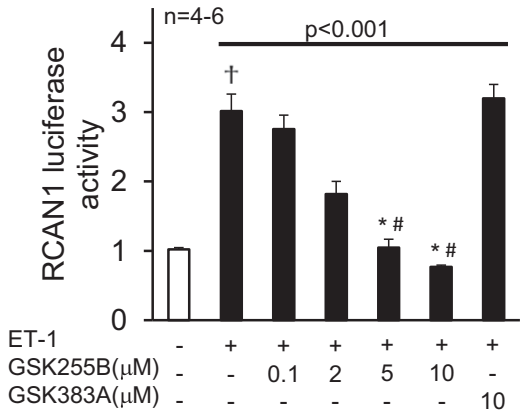

Fig. S1. *Rcan1* luciferase activity in neonatal rat cardiomyocytes stimulated with 0.1 μM endothelin-1 (ET-1) and treated with GSK255B or inactive control (GSK383A). $^{\dagger}P < 0.05$ vs. vehicle control; $^{*}P < 0.05$ vs. vehicle + ET-1; $^{\#}P < 0.05$ vs. inactive control (GSK383A).

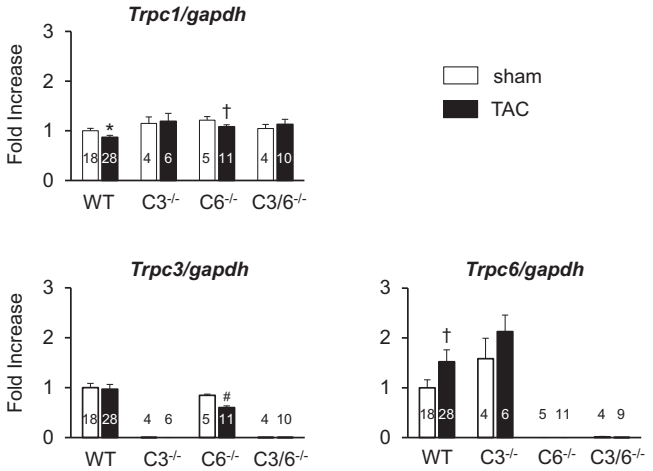

Fig. S2. Gene expression of *Trpc1*, *Trpc3*, and *Trpc6* at rest and after TAC for WT and TRPC3- or TRPC6-selective or double KO genotype. $^{*}P < 0.05$ vs. sham; $^{\#}P < 0.001$ vs. sham; $^{\dagger}P = 0.1$ vs. sham. The numbers of mice employed for each data point is displayed on the graphs.

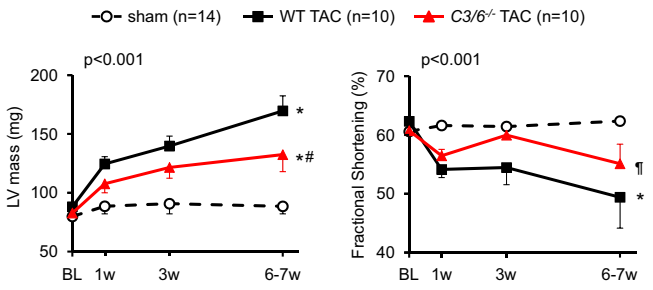

Fig. S3. Echocardiographic analyses of left ventricular mass and fractional shortening in TRPC3/6 double KO mice subjected to 6–7 wk of TAC. *P* values denote (group) × (time) interaction based on ANCOVA; symbols identify the interaction term for pairwise covariance analysis versus sham control ($^{*}P < 0.001$) or WT-TAC ($^{\#}P < 0.001$; $^{\P}P < 0.002$). Sham control data combine the littermate and KO groups, because there was no significant difference between them. Data for baseline (BL) and 1 and 3 weeks after TAC are as shown in Fig. 3*C*, with the addition of the 6–7 week time point shown here.

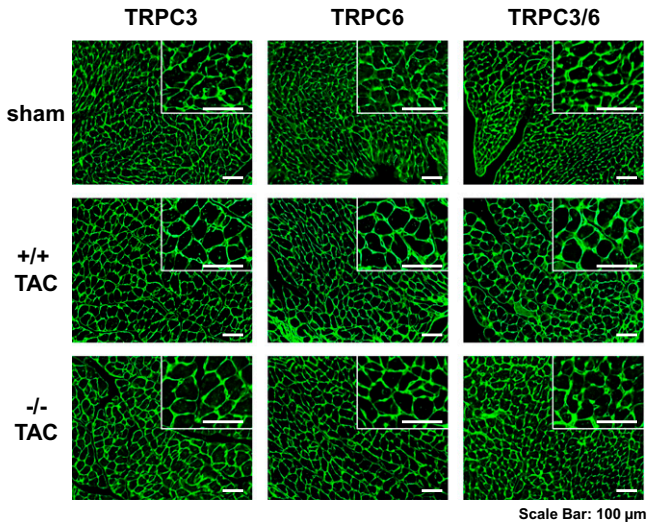

Fig. S4. Representative images of wheat germ agglutinin-stained left ventricular myocardium sections from mice exposed to pressure overload (n = 5–6 per group).

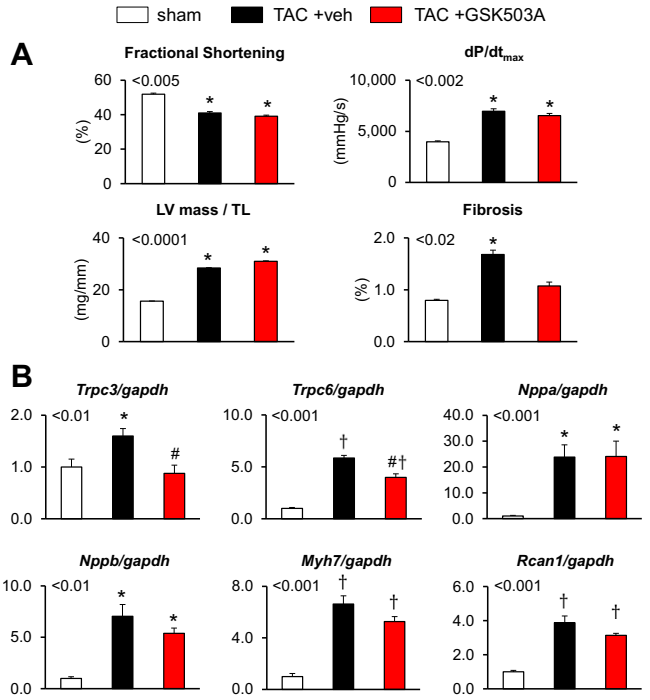

Fig. S5. (*A*) Chronic treatment of rats with GSK503A had no effect on functional parameters (fractional shortening, maximal rate of pressure rise dP/dt_{max}) or interstitial fibrosis. The left ventricular mass normalized to tibia length (TL) was increased in vehicle- and GSK503A-treated TAC animals. (*B*) *Trpc3* and *Trpc6* gene expression increased after aortic banding in rats and was reduced by GSK503A treatment. Molecular heart failure markers (*Nppa*, *Nppb*, and *Myh7*) and *Rcan1* expression were increased in banded hearts, but were not affected by GSK503A treatment. *$P < 0.05$ vs. sham; $^{\#}P < 0.05$ vs. vehicle; $^{\dagger}P < 0.01$ vs. sham. n = 8–10 for molecular studies; n = 10–14 for functional studies and fibrosis.